THE JOURNAL OF BIOLOGICAL CHEMISTRY VOL. 291, NO. 1, pp. 255–265, January 1, 2016
© 2016 by The American Society for Biochemistry and Molecular Biology, Inc. Published in the U.S.A.

Selective Inhibition of Bacterial Tryptophanyl-tRNA Synthetases by Indolmycin Is Mechanism-based*

Received for publication, September 5, 2015, and in revised form, November 3, 2015 Published, JBC Papers in Press, November 9, 2015, DOI 10.1074/jbc.M115.690321

Tishan L. Williams[‡1], **Yuhui W. Yin**[§], **and Charles W. Carter, Jr.**[‡]

From the [‡]*Department of Biochemistry and Biophysics, University of North Carolina, Chapel Hill, North Carolina 27599-7260 and* [§]*Department of Pharmacology and Toxicology, University of Texas Medical Branch, Galveston Texas 77555-0144*

Indolmycin is a natural tryptophan analog that competes with tryptophan for binding to tryptophanyl-tRNA synthetase (TrpRS) enzymes. Bacterial and eukaryotic cytosolic TrpRSs have comparable affinities for tryptophan ($K_m \sim 2\ \mu M$), and yet only bacterial TrpRSs are inhibited by indolmycin. Despite the similarity between these ligands, *Bacillus stearothermophilus* (Bs)TrpRS preferentially binds indolmycin ~1500-fold more tightly than its tryptophan substrate. Kinetic characterization and crystallographic analysis of BsTrpRS allowed us to probe novel aspects of indolmycin inhibitory action. Previous work had revealed that long range coupling to residues within an allosteric region called the D1 switch of BsTrpRS positions the Mg^{2+} ion in a manner that allows it to assist in transition state stabilization. The Mg^{2+} ion in the inhibited complex forms significantly closer contacts with non-bridging oxygen atoms from each phosphate group of ATP and three water molecules than occur in the (presumably catalytically competent) pre-transition state (preTS) crystal structures. We propose that this altered coordination stabilizes a ground state Mg^{2+}·ATP configuration, accounting for the high affinity inhibition of BsTrpRS by indolmycin. Conversely, both the ATP configuration and Mg^{2+} coordination in the human cytosolic (H_c)TrpRS preTS structure differ greatly from the BsTrpRS preTS structure. The effect of these differences is that catalysis occurs via a different transition state stabilization mechanism in H_cTrpRS with a yet-to-be determined role for Mg^{2+}. Modeling indolmycin into the tryptophan binding site points to steric hindrance and an inability to retain the interactions used for tryptophan substrate recognition as causes for the 1000-fold weaker indolmycin affinity to H_cTrpRS.

The accumulation of resistance in pathogenic organisms over time and with prolonged drug use necessitates the continued development of new anti-infective therapeutics. Such developments can include modifications to current drugs that are active against exploited targets while counteracting current resistance mechanisms or novel compounds targeted against underexploited targets. One group of enzyme targets that has been validated but remains underexploited is the class of aminoacyl-tRNA synthetases (aaRSs).[2] Aminoacyl-tRNA synthetases maintain the fidelity of the genetic code by ensuring the charging of tRNA with its cognate amino acid via the following two-step reaction.

$$\text{aaRS} + \text{ATP} + \text{aa} \rightarrow \text{aaRS·aa-AMP} + \text{PPi}$$

REACTION 1

$$\text{aaRS·aa-AMP} + \text{tRNA} \rightarrow \text{aaRS} + \text{aa-tRNA} + \text{AMP}$$

REACTION 2

All aaRS enzymes bind ATP and activate a specific amino acid by catalyzing the formation of an aminoacyl 5′-adenylate (aa-AMP) during the first step. This is followed by transfer of the activated amino acid to the 3′-end of the correct tRNA. Structural and mechanistic differences among the different aaRS enzymes as well as orthologs of individual synthetases make it possible to selectively modulate the activity of specific synthetases, *e.g.* prokaryotic over eukaryotic TrpRS (1). This makes the aaRS enzymes attractive targets for novel anti-infective therapeutics.

Any compounds intended for clinical use must be much less inhibitory against the eukaryotic orthologs of its intended target. Naturally occurring aminoacyl-tRNA synthetase inhibitors include indolmycin (TrpRS), granaticin (LeuRS), mupirocin (IleRS), and ochratoxin A (PheRS) (1–4). Of these, mupirocin displays the required selectivity for prokaryotic over eukaryotic IleRS and has been developed for the treatment of infections in humans (5).

Indolmycin produced by *Streptomyces griseus* displays selective inhibition for prokaryotic TrpRS (9 nM; *Escherichia coli*) over eukaryotic TrpRS (4 mM; *Bos taurus*) (6). Problems with off-target effects on tryptophan metabolism have prevented its clinical use (7). However, if we could understand the molecular basis for the observed inhibition and selectivity we could exploit this information for the rational design of antibiotics targeted against TrpRS on pathogens.

Structurally, tryptophan and indolmycin are quite similar with a heterocyclic indole moiety at the root of each ligand (Fig.

* This work was supported by National Institutes of Health Grant GM90406 through the NIGMS (to C. W. C.) and an NIGMS diversity supplement (to T. W.). The authors declare that they have no conflicts of interest with the contents of this article. The content is solely the responsibility of the authors and does not necessarily represent the official views of the National Institutes of Health.

The atomic coordinates and structure factors (code 5DK4) have been deposited in the Protein Data Bank (http://wwpdb.org/).

[1] To whom correspondence should be addressed. Fax: 919-966-2852; E-mail: tishan.williams@gmail.com.

[2] The abbreviations used are: aaRS, aminoacyl-tRNA synthetase; TrpRS, tryptophanyl-tRNA synthetase; Bs, *B. stearothermophilus*; H_c, human cytoplasmic; LTN, tryptophanamide; IND, indolmycin; PreTS, pre-transition state; Bt, *B. taurus*; TEV, tobacco etch virus; OXA, methylamino-substituted oxazolinone ring.

Downloaded from http://www.jbc.org/ at DOE/SC/OSTI on March 11, 2020

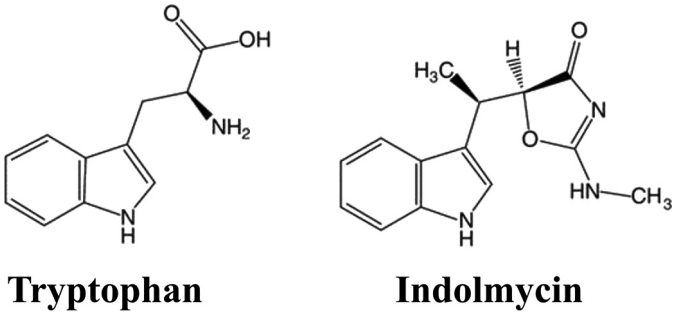

FIGURE 1. **Functional equivalences of tryptophan and indolmycin.** Indolmycin differs from tryptophan in three key ways: 1) the incorporation of Cα constituents into an oxazolinone ring, 2) a methylamino group extending from the oxazolinone ring, and 3) replacement of a hydrogen on Cβ with a hydrophobic methyl group.

1). Indolmycin differs from tryptophan in the following ways. (i) The carbon that is functionally equivalent to Cβ is substituted with a methyl group. (ii) The carbonyl carbon is part of an oxazolinone ring. (iii) The hydroxyl and amine groups of tryptophan are replaced by the nitrogen and oxygen atoms of the oxazolinone ring, respectively. (iv) The -NH-CH3 moiety attached to the oxazolinone ring does not have functionally equivalent atoms in tryptophan.

BsTrpRS is one of the most extensively characterized TrpRS enzymes. Mechanistically a Mg^{2+} ion is linked to what appears to be a dissociative transition state for tryptophan activation (8–10). During catalysis, the Mg^{2+} ion helps compensate for the increased negative charge that develops on the PP_i leaving group, resulting from breaking the αP–O–βP bond. The Mg^{2+} ion must move to be catalytically competent, but no protein-metal interactions have been observed in any of the BsTrpRS crystal structures determined. Instead, a remote allosteric location, the D1 switch, must undergo significant conformational change to promote the Mg^{2+} ion to a catalytically competent position. The metal moves closer to the PP_i leaving group, whose charge is further stabilized in the transition state by the KMSKS loop. ATP binding is required for the conformational switching between the open and closed states that allows for catalysis. ATP-dependent induced fit closing of the active site brings ATP ~4 Å closer to tryptophan in a predominantly translational movement mediated by relative movement of the catalytic and anticodon-binding domains.

In the absence of ATP, tryptophan binding is promoted by hydrophobic van der Waals interactions, π-π interactions with Phe^{5}, and a hydrogen bond between the indole nitrogen and Asp^{132} of the specificity helix. When both substrates bind, the tryptophan substrate undergoes a rotational movement that brings the indole ring deeper into the binding pocket and results in more stabilizing interactions between tryptophan and active site residues. This change is facilitated by the inward movement of the specificity helix that is not observed when only tryptophan is bound.

ATP-dependent induced fit rearrangement of the active site facilitates proper ATP positioning in BsTrpRS, and molecular dynamics simulations demonstrate that tryptophan is required to achieve the requisite movement of the αP in H_cTrpRS (11, 12). Even a modest substitution of tryptophanamide in place of tryptophan prevents the repositioning of ATP. These findings support the idea that H_cTrpRS is intrinsically better at discriminating between tryptophan and its structural analogs than is BsTrpRS.

H_cTrpRS uses different structural elements for substrate recognition than its prokaryotic orthologs (13). Such elements include an extended N terminus with a β1-β2 hairpin structure shown to have a role in ATP binding as well as the amino acid activation reaction in H_cTrpRS (14). In contrast to BsTrpRS, it is tryptophan binding that leads to induced fit rearrangement of the active site in H_cTrpRS. There are a greater number of binding determinants for tryptophan recognition as eight direct and water-mediated hydrogen bonds with polar side chains stabilize tryptophan in the active site. It has been proposed that amino acid activation proceeds via an associative transition state in H_cTrpRS with an unclear role of Mg^{2+} in the catalytic transition state (11). However, comparison of the pre-transition (Protein Data Bank code 2QUI) and product states (Protein Data Bank code 2QUJ) shows that, as with BsTrpRS, the αP of ATP must move 5.3 Å to be in a position for nucleophilic attack by tryptophan.

Despite mechanistic and structural differences, BsTrpRS and H_cTrpRS have comparable tryptophan binding affinities. However, these inherent differences between prokaryotic and eukaryotic TrpRS enzymes promote the binding of indolmycin to prokaryotic TrpRSs ~1500-fold while protecting eukaryotic TrpRSs from such inhibition by a comparable amount. Determining the structure of BsTrpRS bound by Mg^{2+}·ATP and indolmycin allowed us to probe the structural basis for indolmycin inhibition and selectivity. Specifically, we examined this structure along with the catalytically relevant structures of BsTrpRS and H_cTrpRS deposited in the Protein Data Bank to answer the following questions. 1) What are the structural consequences of binding indolmycin? 2) Why is indolmycin a tight inhibitor of prokaryotic TrpRS? 3) Why is indolmycin not an inhibitor of eukaryotic cytosolic TrpRSs?

Experimental Procedures

Construction of pet28-His-BsTrpRS Vector—The full-length BsTrpRS sequence was PCR-amplified from a pet11 construct made previously in the laboratory. PCR primers contained restriction sites for BamHI and HindIII. The resultant PCR product was digested with BamHI and HindIII. A three-way ligation among the PCR product (BamHI/HindIII), double-stranded oligo encoding for the TEV site (NdeI/BamHI), and pet28b (NdeI/HindIII) yielded an expression vector for His-TEV-BsTrpRS.

Expression and Purification of His-BsTrpRS—BsTrpRS was expressed by autoinduction with BL21(DE3)pLysS cells at 37 °C (15). The cells were pelleted at 4500 rpm for 30 min, resuspended in lysis buffer, and frozen at −20 °C. Upon thawing, cells were sonicated and centrifuged (16,000 rpm, 4 °C, 1 h). His-BsTrpRS was captured from the lysate on nickel-nitrilotriacetic acid resin and eluted with 0.3 M imidazole. Purified protein was cleaved overnight with TEV while dialyzing out the imidazole. The cleaved protein mixture was passed back over a nickel-nitrilotriacetic acid column to capture both uncleaved protein and His-TEV protease.

Active Site Titration—Active sites were titrated by following the loss of ATP to determine the fraction of molecules compe-

Downloaded from http://www.jbc.org/ at DOE/SC/OSTI on March 11, 2020

tent for catalysis (16, 17). The reaction was performed at 37 °C in a final reaction mixture containing 5000 cpm/μl [γ-^{32}P]ATP, 10 μM ATP, 0.5 mM tryptophan, 5 mM $MgCl_2$, and 0.05 unit/μl inorganic pyrophosphatase. The reaction was initiated with enzyme at a final concentration of 3 μM. At various time points between 10 s and 30 min, 3 μl of the reaction were added to 6 μl of quench buffer (sodium acetate, pH 5.3, 1% SDS) and placed on ice. Three microliters of each quenched reaction were spotted onto a cellulose-PEI TLC plate and run in 0.75 M KH_2PO4, pH 3.5 with 4 M urea to separate $^{32}P_i$ and [γ-^{32}P]ATP. Plates were developed using a Typhoon imager and analyzed with ImageJ (18) and JMP (19).

Michaelis-Menten Kinetics—The incorporation of [^{32}P]PP_i into ATP was tracked either by TLC or filter binding after purification on charcoal (17). Reactions contained [^{32}P]PP_i (5000 cpm/μl for TLC and 400 cpm/μl for the filter assay), 0.1 M Tris, pH 8.0, 70 mM β-mercaptoethanol, 5 mM $MgCl_2$, 10 mM KF, 2 mM PP_i, 2 mM ATP, and tryptophan ranging from 0.3 to 100 μM. Reactions were initiated with enzyme at a final concentration of 30 nM.

Indolmycin Inhibition Assays—Inhibition assays were performed as described above; Michaelis-Menten experiments for tryptophan were performed in the presence of stoichiometric amounts of indolmycin (a gift from Pfizer, ca. 1994) to enzyme. Indolmycin to enzyme ratios of 1:5, 1:1, and 5:1 were used, and results were fitted to a competitive inhibition model (1) using JMP (19). Non-linear regression to Equation 1 allowed for determination of K_m for tryptophan and K_i for indolmycin.

$$\text{Rate} = \frac{[\text{Tryptophan}] \times k_{\text{cat}}}{\left(1 + \frac{[\text{Indolmycin}]}{K_i} + [\text{Tryptophan}]\right)} \quad \text{(Eq. 1)}$$

Differential Scanning Fluorimetry (Thermofluor)—The effects of ATP, tryptophanamide (LTN), and indolmycin on the thermal stability of BsTrpRS were assessed by thermofluor. We showed separately[3] that differential scanning fluorimetry detects a conversion of TrpRS into a molten globule form that fully denatures only at higher temperature. The following saturating ligand concentrations were used to ensure a predominance of conformations corresponding to those observed in crystal structures: 5 mM ATP, 5 mM $MgCl_2$, 10 mM LTN, and 600 μM indolmycin. All reactions contained 8 μM BsTrpRS, 50 mM NaCl, 5 mM β-mercaptoethanol, 50 mM Hepes, pH 7.5, and 0.15% SYPRO Orange in a final volume of 20 μl. Fluorescence intensities were determined using an Applied Biosystems 7900HTFast Real Time PCR instrument, and data were analyzed with MATLAB (Mathworks) with routines developed by Visinets, Inc. The software was built as a pipeline of several m-files connected to provide full analysis of the data, including thermodynamic characterization and presentation of statistics. Fluorescence at each data point along a melting curve is assumed to be the sum of contributions from two states with probabilities p_1 and p_2 established by thermodynamic equilibrium between the two states.

$$F(t) = (a_1 + b_1T) \times p_1 + (a_2 + b_2T) \times p_2 \quad \text{(Eq. 2)}$$

where a_1 and a_2 are adjustable parameters representing intercepts, b_1 and b_2 are the slopes of the linear dependences of the initial and final states, and T is the Kelvin temperature. The pipeline consists of the following three parts.

Part A is reading the data from high throughput, 384-well, real time PCR files and transforming them into a matrix consisting of four columns: (i) number of the well from which temperature-dependent readings were taken, (ii) an index representing the protein variant, and finally the data, (iii) temperature and (iv) fluorescence readings.

Part B is fitting the thermofluor data to a thermodynamic model (Equations 3 and 4).

$$F = F_0 + \frac{a_1 + b_1T + (a_2 + b_2T)e^{-\Delta G(T)/RT}}{1 + e^{-\Delta G(T)/RT}}$$

$$= F_0 + (a_2 + b_2T) + \frac{(a_1 - a_2) + (b_1 - b_2)T}{1 + e^{-\Delta G(T)/RT}} \quad \text{(Eq. 3)}$$

where ΔG is the Gibbs energy difference between the two states and $e^{-\Delta G(T)/RT}$ is the Boltzmann factor that determines the state probabilities p_1 and p_2.

$$\Delta G = \Delta H(T_m) + \Delta c_p \times (T - T_m) - T\left[\Delta S(T_m) + c_p \ln\left(\frac{T}{T_m}\right)\right] \quad \text{(Eq. 4)}$$

where ΔH and ΔS are the enthalpy and entropy changes between the states, c_p is the heat capacity at temperature T, and Δc_p is the heat capacity change between the two states at the melting temperature T_m.

Part C is independent determination of T_m assuming that the state probabilities p_1 and p_2 can be estimated from distances between the intersection of the melting curve with vertical lines connecting the extrapolated linear final and initial slopes. Data initially worked up using both methods B and C agreed closely, and the analysis reported here follows C.

Crystallization, Data Collection, and Structure Determination—Crystals of seleno-Met-substituted BsTrpRS in complex with ATP, Mg^{2+}, and indolmycin were grown by vapor diffusion against a reservoir of 1.4 M potassium citrate and 0.1 M Hepes, pH 7.4. Crystals were cryoprotected in Fomblin-Y and passed in a nitrogen airstream before plunging into liquid nitrogen. Data were collected remotely at Southeast Regional Collaborative Access Team (Beamline ID-22) using inverse beam geometry at 0.979 Å to obtain experimental phases from the Bijvoet differences and processed with XDS (20). PHENIX (21) and Coot (22) were used for phase determination, to interpret the map, and to iteratively refine the final structure (Protein Data Bank code 5DK4).

Results

BsTrpRS Binds Indolmycin ~1500× More Tightly than Tryptophan—Indolmycin is a competitive inhibitor of *Bacillus stearothermophilus* and other bacterial TrpRS enzymes that competes with tryptophan for binding to the active site of the enzyme. By conducting Michaelis-Menten experiments at

[3] V. Weinreb and G. Weinreb, unpublished data.

Downloaded from http://www.jbc.org/ at DOE/SC/OSTI on March 11, 2020

TABLE 1

Steady-state kinetic analysis of indolmycin inhibition

Non-linear regression analysis of 64 data points from steady-state kinetics experiments confirms indolmycin as a tight binding competitive inhibitor of BsTrpRS. PP_i exchange assays performed in the presence of saturating Mg^{2+}·ATP with varying concentrations of tryptophan and indolmycin show that BsTrpRS binds indolmycin ~1450 times more tightly than tryptophan. The difference in free energy between the catalytic and inhibited complexes is ~4.5 kcal/mol.

k_{cat}	ΔG_{kcat}	$K_{m,tryptophan}$	ΔG_{Km}	$K_{i,indolmycin}$	ΔG_{Ki}	$K_{m,tryptophan}/K_{i,indolmycin}$
s^{-1}	*kcal/mol*	M	*kcal/mol*	M	*kcal/mol*	
31.6 ± 0.8	−2.1 ± 0.01	3.0E−06 ± 6.4E−07	7.8 ± 0.1	2.0E−09 ± 5.2E−10	12.3 ± 0.1	1.5E+03

increasing tryptophan concentrations in the presence of different indolmycin concentrations and fitting all 64 data points simultaneously to Equation 1, we were able to determine $K_{m,tryptophan}$ (3 μM) and $K_{i,indolmycin}$ (2 nM) (Table 1). As these experiments were carried out under exchange conditions (23), we determined the standard free energy, $\Delta G^0 = -RT\ln K$, at 310 K for tryptophan and indolmycin binding to be 7.8 and 12.3 kcal/mol, respectively. This translates to a free energy difference of 4.5 kcal/mol between the affinities of the catalytic and inhibited complexes for the indole-containing ligand. To determine what factors account for the observed difference in binding free energy, we determined the structure of the BsTrpRS·ATP·indolmycin ternary complex and then conducted differential scanning fluorimetric experiments in the presence of various ligands.

Indolmycin and ATP Form a Ternary Complex with BsTrpRS—Extensive crystallization studies conducted on BsTrpRS have revealed three distinct conformational states: an open conformation (ligand-free, tryptophan, low ATP (12, 24)), a closed pre-transition state (high ATP, ATP + tryptophanamide (9, 12)), and a closed product conformation (Trp-5′-AMP (25, 26)).

A previously unpublished structure of BsTrpRS bound to Mg^{2+}·ATP and indolmycin was never deposited (27). Nevertheless, that structure was the first example of a series of subsequently solved structures that have been described as "pre-transition state" (PreTS) structures (Protein Data Bank codes 1MAU and 1M83 (12)). In these structures, the initial ATP binding site in the small domain composed of the N-terminal α-helix and the anticodon-binding domain closes on the remainder of the Rossmann fold, bringing the nucleotide α-phosphate from 6.7 Å away to within van der Waals contact distance of the tryptophan carboxyl oxygen (12).

The new structure presented here is at higher resolution (1.9 *versus* 2.4 Å), and the experimental phases greatly enhanced the quality of electron density maps (Table 2 and Fig. 2). Details of the new structure, such as the orientation of the ribose and the metal position, are quite similar to those observed in deposited PreTS structures 1MAU and 1M83. Detailed differences that appear functionally relevant are discussed below.

Indolmycin Induces New Contacts with Active Site Side Chains—Indolmycin makes contacts with the side chains of His^{43}, Asp^{132}, and Gln^{147} as well as two water molecules (Fig. 3*A*). The interaction between Oδ2 of Asp^{132} in the specificity helix and the nitrogen atom of the indole ring is observed when tryptophan (3.1 Å), tryptophanamide (3.0 Å), or indolmycin (2.9 Å) is bound. The addition of the oxazolinone group to the ligand allows for stabilizing interactions with His^{43} and Gln^{147} with functionalities on either side of the ring, which have the effect of fixing the rotation of the ring (Fig. 3*B*). Nδ1 of His^{43} can donate and/or accept a hydrogen bond from N2 (methylamino group) of indolmycin. In addition to these hydrogen bonds, His^{43} can form a salt bridge with Oδ2 of Asp^{132} (2.8 Å). The amide group of Gln^{147} forms two hydrogen bonds, one with the carbonyl oxygen of the oxazolinone ring (3.0 Å) and another with Oδ2 of Asp^{146} (3.0 Å). Oδ1 of Asp^{146} makes a highly conserved hydrogen bond with the 2′-OH group of ATP (2.7 Å). These side chain interactions in the conserved GEDQ motif link the indolmycin and ATP binding sites while reinforcing the linkage between opposite sides of the indole-binding pocket.

TABLE 2

Data collection and refinement statistics for crystals of the BsTrpRS·indolmycin·Mg^{2+}·ATP complex

Crystallographic data, including experimental phases, of selenomethionylated BsTrpRS crystals were collected on Beamline ID-22. The final structure was determined to 1.9-Å resolution and refined to an R_{work}/R_{free} of 16.9/18.9%. r.m.s., root mean square.

Data collection	
Space group	$P4_32_12$
Cell constants	
a, b, c (Å)	62.04, 62.04, 219.06
α, β, γ (°)	90.00, 90.00, 90.00
Resolution (Å)	43.02–1.9
Completeness (%)[a]	99.7 (97.9)
CC1/2 (%)[a,b]	99.6 (93.2)
R_{meas} (%)[a]	15.3 (61.9)
Mean $I/\sigma I$[a]	12.6 (3.3)
Number of reflections	464,942
Multiplicity	15.5
Refinement	
R_{work}/R_{free} (%)	16.6/18.7
F_o, F_c correlation	0.96
r.m.s. bonds	0.005
r.m.s. angles	0.994
Ramachandran favored (%)	97.0
Ramachandran outliers (%)	0.0
Average B, all atoms (Å^2)	32.0
Clash score	2.2
Protein Data Bank code	5DK4

[a] Highest resolution shell is shown in parentheses.
[b] CC1/2 is the percentage of correlation between intensities from random half-data sets.

Structurally, indolmycin binding also prevents the Tyr^{125} rotamer switch that occurs upon the enzyme going from its open to closed conformation (Fig. 4, *A* and *B*). During the catalytic cycle, Tyr^{125} changes hydrogen-bonding partners from His^{150} (2.7 Å) in the open conformation to the α-amino group (2.4 Å) of the tryptophan substrate in the closed PreTS. The tryptophanyl-adenylate intermediate is stabilized by two polar contacts with the hydroxyl group of Tyr^{125} (Protein Data Bank code1I6K). The inhibited state maintains the side chain interaction between Tyr^{125} and His^{150} (2.8 Å) observed in the open state.

Structural Modifications Induced by Indolmycin to the Mg^{2+}·ATP Configuration—Superposition of the inhibited structure onto the closed PreTS structure (Protein Data Bank code 1MAU) gives a root mean square deviation of 0.28 Å for 323 Cα pairs. For comparison, the two closed PreTS structures,

Downloaded from http://www.jbc.org/ at DOE/SC/OSTI on March 11, 2020

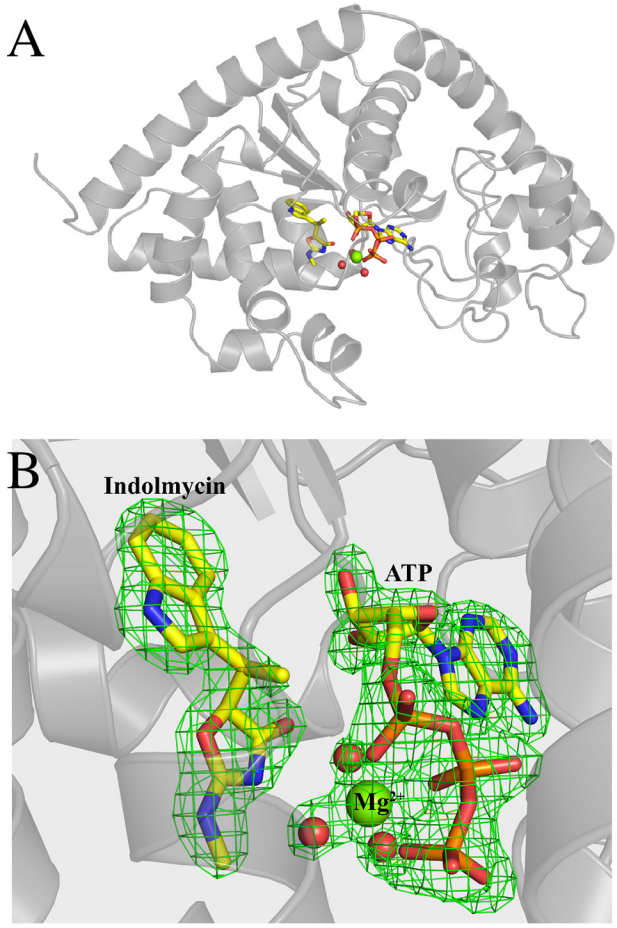

FIGURE 2. **BsTrpRS forms a ternary complex with indolmycin and Mg^{2+}·ATP in a closed conformation.** *A*, functionally dimeric BsTrpRS crystallizes with one monomer in the asymmetric unit. *B*, in addition to indolmycin and ATP, the active site contains a Mg^{2+} ion and three stable water molecules. The $F_o - F_c$ omit map, derived by omitting indolmycin, ATP, Mg^{2+}, and three water molecules from a final round of refinement, contoured to 4.0 σ is depicted in *green*.

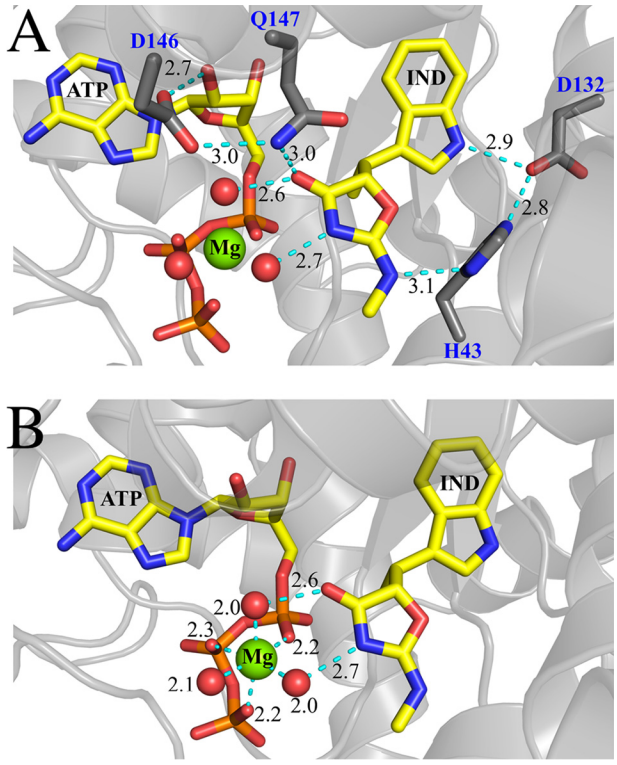

FIGURE 3. **Hydrogen bonding and electrostatic interactions promote indolmycin binding and Mg^{2+} coordination within the active site.** *A*, BsTrpRS residues His^{43}, Asp^{132}, and Gln^{147} make stabilizing contacts with IND via side chain atoms. The ATP and indolmycin binding subsites are linked via a hydrogen bond (2.7 Å) between Asp^{146} and Gln^{147} of the conserved G*X*DQ motif. *B*, Mg^{2+} forms tight electrostatic interactions (2.0–2.3 Å) with three water molecules (*red spheres*) and an oxygen atom from each phosphate group of ATP. Two of these water molecules are within hydrogen bonding distance (2.6 and 2.7 Å) of indolmycin.

1MAU and 1M83, have a root mean square deviation 0.17 Å for 328 Cα pairs. The greatest structural difference between the PreTS and inhibited states occurs around Glu^{103}–Ala^{120} with a root mean square deviation of 0.63 Å for these 18 residues. This mobile loop, which contains Gln^{107} and Lys^{111}, is more open by ~0.5 Å in the inhibited structure as measured from the γP of ATP to the α-carbons of residues Gln^{107}, Lys^{111}, and Lys^{115}. The carbonyl oxygen of the Gln^{107} side chain accepts a hydrogen bond from the water molecule coordinated to the Mg^{2+} ion (2.8 Å) and another from Nϵ2 of Gln^{147} (3.0 Å) in the pre-transition state. Steric clashing with the constrained Tyr^{125} rotamer prevents Gln^{107} from switching rotamers in the inhibited state. As such, the interaction with Gln^{147} is not observed. Instead, the side chain of Gln^{107} accepts a hydrogen bond at Oϵ1 from a water molecule (3.0 Å) and donates a hydrogen bond at Nϵ2 to another water molecule (3.3 Å).

In the pre-transition state, the Nζ atom of Lys^{111} forms a salt bridge with the Oγ1 atom of ATP (2.9 Å), which also forms a strong electrostatic interaction with the catalytic Mg^{2+} ion (2.4 Å). This interaction presumably is important for stabilizing the developing charge on the PP_i leaving group released after tryptophan activation. Additionally, in the pre-transition state, Lys^{111} is in position to act as a hydrogen bond donor to the one water molecule coordinated to the Mg^{2+} ion (Fig. 5). The subtle opening of this loop in the inhibited state weakens the salt bridge between the Lys^{111} Nζ atom and the Oγ1 atom of ATP (3.4 Å) from that observed in the preTS. Now the closest interactions are with three water molecules (2.6, 2.8, and 2.8 Å), none of which are coordinated directly to the catalytic Mg^{2+} ion so they are not shown in Fig. 5.

Replacement of tryptophan(amide) with indolmycin in the active site alters the coordination and placement of the Mg^{2+} ion used during the activation step of the aminoacylation reaction. Presumably because its orientation is fixed by the hydrogen bonding network described above, the oxazolinone forms hydrogen bonds with two water molecules. Introduction of these two water molecules is associated with the movement of the Mg^{2+} ion into a hexavalent coordination that closely resembles stable configurations generated in quantum mechanical simulations of Mg^{2+}·ATP.[4]

As is also true in the PreTS structure, the Mg^{2+} ion in the inhibited BsTrpRS structure coordinates with a non-bridging oxygen from each phosphate group and three water molecules (Figs. 3*B* and 4*B*), two of which are further stabilized by the presence of indolmycin. In addition to the three electrostatic interactions with ATP, only one water molecule was seen to

[4] S. Liu, unpublished data.

Downloaded from http://www.jbc.org/ at DOE/SC/OSTI on March 11, 2020

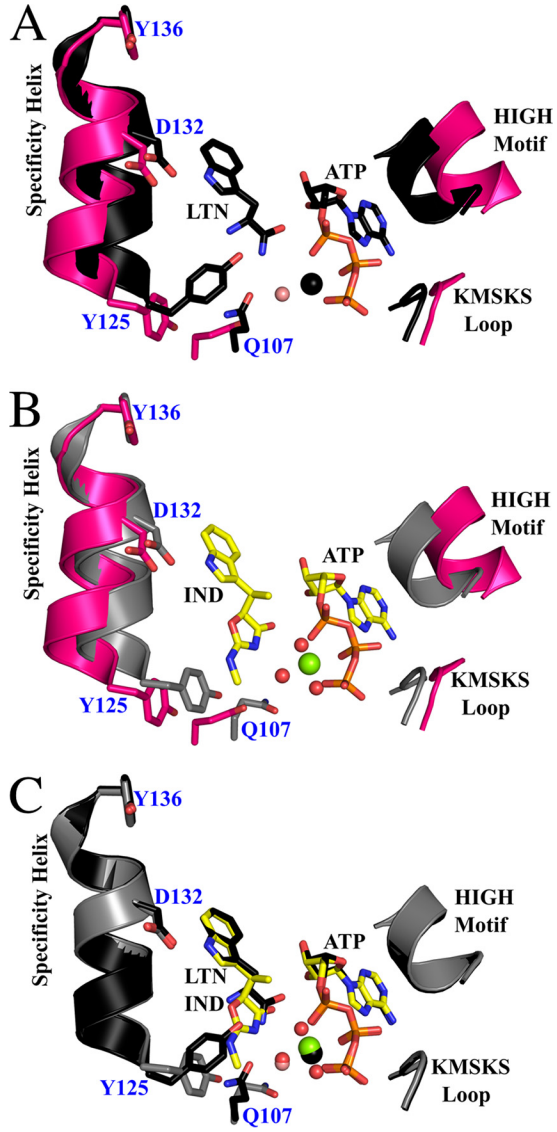

FIGURE 4. **Comparison of ligand-free, preTS, and inhibited BsTrpRS structures.** *A*, compared with the apo form (*pink*; Protein Data Bank code 1D2R), the fully occupied PreTS structure (*black*; Protein Data Bank code 1MAU) assumes a closed conformation. The Cα of Tyr^{125} is shifted inward by 2.4 Å, and the side chain is flipped ~45° (measured from OH-Ca-OH). A Mg^{2+} ion (*black sphere*) forms electrostatic interactions with ATP and one water molecule (*salmon sphere*). *B*, binding of indolmycin and ATP causes similar shifts in the backbone (*gray*) as the enzyme adopts a closed conformation. However, due to the addition of the methylamino-substituted oxazolinone ring, this movement to the closed conformation is not accompanied by a rotamer change of Tyr^{125} in the inhibited structure. *C*, consequently, Gln^{107} is constrained and is rotated 106° around Cβ away from the specificity helix in the inhibited state compared with the pre-transition state. Finally, the Mg^{2+} (*green sphere*) is shifted toward the αPO_4 and has hexavalent coordination to ATP and three water molecules (*red spheres*) as compared with the preTS structure.

coordinate with the Mg^{2+} ion in the PreTS structure (Protein Data Bank code 1MAU) (Figs. 4*A* and 5). The side chain residues that accept and donate hydrogen bonds to this water molecule differ between these two states (Fig. 5). Due to the different Gln^{107} rotamer and slight opening of the mobile loop around Lys^{111}, these two residues no longer interact with this water molecule in the inhibited state.

The Mg^{2+} ion is closer and more central to the triphosphate moiety in the inhibited structure than in the PreTS structure

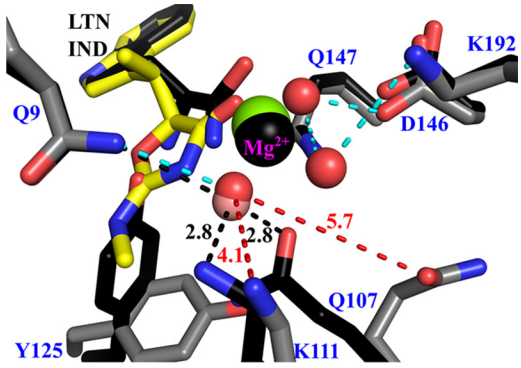

FIGURE 5. **Differential BsTrpRS side chain interactions with the water molecules electrostatically coordinated with Mg^{2+} in the PreTS and inhibited structures.** Gln^{9}, Gln^{107}, and Lys^{111} are in position to accept (Gln^{107}) or donate (Gln^{9} and Lys^{111}) hydrogen bonds (*black dashed lines*) to the water molecule (*salmon sphere*) coordinated with Mg^{2+} (*black sphere*) in the PreTS (*black sticks*). As indolmycin binding leads to opening of the mobile loop containing Gln^{107} and Lys^{111}, these residues are too far (*red dashed lines*) to form stabilizing interactions with the equivalent water molecule (*red sphere*) in the inhibited complex (*gray sticks*). The three water molecules (*red spheres*) electrostatically coordinated to Mg^{2+} (*green sphere*) in the inhibited complex are stabilized by interactions (*cyan dashed lines*) with side chain atoms of residues Gln^{9}, Asp^{146}, Gln^{147}, and Lys^{192}.

(Fig. 4*C*) and makes equivalent interactions with the phosphate oxygen atoms. The significance of the differences in metal positions is evident from several measurements. (i) Metal to oxygen distances are significantly shorter (0.2 Å; $p = 0.002$) in the inhibited complexes. (ii) Movement of the divalent metal ion into closer contact with the ATP phosphate oxygen atoms is associated with a subtle but statistically significant opening of the active site crevice among the N-terminal helix of the second crossover connection (the G*X*DQ motif), the KMSKS signature, and the mobile loop containing Lys^{111}.

Ligand-induced Stability Changes Imply Cooperative Sources of High Indolmycin Affinity—The nature of the ligands within the active site has a significant effect on the conformation and thermal stability of an enzyme. For small perturbations, the fractional change in melting temperature ($\Delta T_m/T_m$) induced by ligand binding is proportional to the free energy change in stability, the proportionality constant being the enthalpy change (ΔH) (28). We use this implicit relationship to assess the stabilizing or destabilizing effects of various ligands on the BsTrpRS enzyme. Binding of ATP, tryptophan, or tryptophanamide stabilizes the thermal transition of molten globule formation by 3, 7, and 7%, respectively (Table 3). Indolmycin enhances the thermal stability of BsTrpRS by 20%, increasing T_m by 13.5 °C. The enhanced affinity for indolmycin over tryptophan results in a shift by 8 °C to higher temperature in the thermal transition due to molten globule formation in the presence of indolmycin compared with tryptophan.

The linkage between protein stability and ligand binding (29–31) implies that we can attribute differences in stability changes to binding affinity. Two of the stabilizing interactions formed between indolmycin and Mg^{2+}-coordinated water molecules are associated with a change in the metal position relative to the ATP phosphate oxygen atoms. A key implication of the structural observations in Figs. 3*A* and 4*C* is that binding of indolmycin to BsTrpRS should be potentiated by the presence of Mg^{2+}·ATP.

Downloaded from http://www.jbc.org/ at DOE/SC/OSTI on March 11, 2020

TABLE 3

Thermofluor analysis of ligand-dependent stability

Differential scanning fluorimetric analysis of ligand-dependent thermal stability of BsTrpRS revealed a stabilizing interaction between indolmycin and ATP via Mg^{2+}. Substrates (ATP and tryptophan) and substrate analogs (LTN and IND) induce conformational changes in BsTrpRS. These changes vary with ligand type and confer varying degrees of thermal stability in the transition to molten globule formation. ATP, tryptophan, tryptophanamide, and indolmycin separately enhance the thermal stability of BsTrpRS. Mg^{2+} is required for additional stabilization by ATP of both LTN-bound and IND-bound BsTrpRS. The inhibited complex (BsTrpRS bound with IND and Mg^{2+}·ATP) is the most thermally stable with a T_m 18.4 and 10.7 °C higher than that of ligand-free (LF) enzyme and PreTS complex, respectively. n/a, not applicable.

Ligand	Mg^{2+}	T_m	ΔT_m	$(\Delta T_m/T_m) \times 100$
		℃	℃	%
LF	−	69.0 ± 0.2	n/a	n/a
ATP	−	71.1 ± 0.1	2.1 ± 0.2	3.0 ± 0.2
TRP	−	74.7 ± 0.1	5.7 ± 0.3	8.2 ± 0.4
LTN	−	74.1 ± 0.1	5.1 ± 0.3	7.4 ± 0.4
LTN + ATP	−	74.7 ± 0.2	5.7 ± 0.2	8.3 ± 0.3
IND	−	82.5 ± 0.2	13.5 ± 0.3	19.6 ± 0.5
IND + ATP	−	83.3 ± 0.3	14.3 ± 0.4	20.7 ± 0.6
LF	+	69.0 ± 0.1	n/a	n/a
ATP	+	71.2 ± 0.03	2.2 ± 0.1	3.1 ± 0.2
TRP	+	74.1 ± 0.1	5.1 ± 0.1	7.4 ± 0.1
LTN	+	74.2 ± 0.2	5.1 ± 0.2	7.4 ± 0.3
LTN + ATP	+	76.8 ± 0.2	7.7 ± 0.1	11.2 ± 0.2
IND	+	82.7 ± 0.04	13.6 ± 0.2	19.7 ± 0.3
IND + ATP	+	87.5 ± 0.1	18.4 ± 0.2	26.7 ± 0.4

The presence/position of Mg^{2+} in the active site is strictly dependent on ATP because the protein makes no contacts with the metal. As no direct ATP-indolmycin interactions are observed, we therefore expected that ATP would enhance the thermal stability of the BsTrpRS·indolmycin complex by a larger amount in the presence compared with the absence of Mg^{2+}. Additionally, we did not expect Mg^{2+} to contribute to thermal stability in the absence of ATP. As expected, the differential scanning fluorimetry measurements show that the BsTrpRS in complex with indolmycin and Mg^{2+}·ATP has a 27% increase in melting temperature compared with ligand-free enzyme with Mg^{2+}·ATP contributing an additional 5 °C of thermal stability on top of the 13.5 °C provided by indolmycin binding. By contrast, binding of indolmycin, indolmycin + Mg^{2+}, or indolmycin + ATP all elicit far smaller changes of ~20% in thermal stability, demonstrating that both Mg^{2+} and ATP are required to confer additional thermal stability to the BsTrpRS·indolmycin (IND) complex.

The conclusion that the metal is essential to the enhanced affinity of indolmycin to the pre-transition state complex can also be derived using the three-dimensional thermodynamic cycle of contributions to stability from ATP, the methylamino-substituted oxazolinone ring (OXA), and the presence/absence of Mg^{2+} (Fig. 6). Differences in binding and thermal stability between tryptophanamide and indolmycin were attributed to the methylamino-substituted oxazolinone ring as this is the major structural difference between these two ligands.

Stabilizing and destabilizing interactions are distinguished by positive and negative non-additivity, respectively. If thermal stability were unaffected by interactions between the ligands, then we expect the effects of binding multiple ligands, *e.g.* ATP and LTN, to be additive and the effects of binding one ligand not to be affected by the presence of a second ligand, thus giving Equations 5 and 6.

$$\Delta T_m(\text{ATP}) + \Delta T_m(\text{LTN}) = \Delta T_m(\text{ATP} + \text{LTN}) \quad \text{(Eq. 5)}$$

$$\Delta T_m(\text{LTN}) = T_m(\text{LTN}) - T_m(\text{LF}) = T_m(\text{ATP} + \text{LTN}) - T_m(\text{ATP}) \quad \text{(Eq. 6)}$$

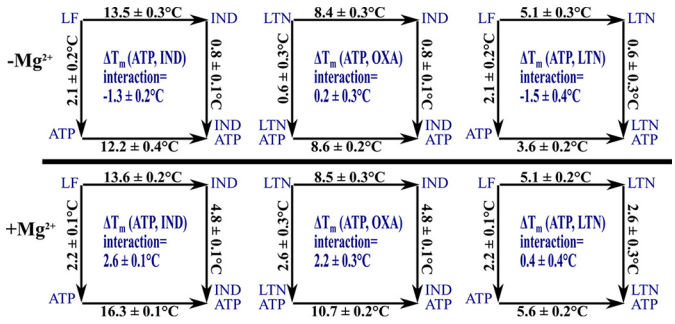

FIGURE 6. **Contributions of Mg^{2+}, ATP, indolmycin, and tryptophanamide to the thermal stability of BsTrpRS.** TrpRS enzymes require a Mg^{2+} ion for tryptophan activation. Although Mg^{2+} does not change the thermal stability of BsTrpRS on its own, its presence or absence significantly impacts the interaction of ATP with both LTN and IND. In the absence of Mg^{2+} (*top row*), both the ATP-LTN and ATP-IND interactions lower the fractional change in T_m by 2% from its expected value. In the presence of Mg^{2+} (*bottom row*), the interaction between ATP and LTN is insignificant, whereas the ATP-IND interaction raises the T_m 4% higher than expected. As expected from the crystal structure, the Mg^{2+}-dependent ATP-IND interaction is mediated through the oxazolinone moiety of indolmycin. *LF*, ligand-free.

An interaction between the ligands would introduce a term, $\Delta T_{m,\text{int}}$, to describe the non-additivity (32), giving Equation 7.

$$\Delta T_m(\text{ATP}) + \Delta T_m(\text{LTN}) + \Delta T_{m,\text{int}} = \Delta T_m(\text{ATP} + \text{LTN}) \quad \text{(Eq. 7)}$$

In the absence of Mg^{2+}, there is no significant ATP-OXA interaction, and binding either IND or LTN reduces the effect of ATP on T_m by ~1.5 °C. The ATP-LTN and ATP-IND interactions are both destabilizing; *i.e.* the doubly liganded complexes melt at lower temperatures. In contrast, addition of Mg^{2+} stabilizes the interactions of ATP with LTN and IND to varying degrees. In the case of LTN-ATP, addition of Mg^{2+} compensates for the destabilizing ATP-LTN interaction such that the interaction is no longer significant. The metal compensates for the −1.3 °C destabilizing ATP-IND interaction and allows for an additional stabilizing interaction of 2.6 °C. Thus, the ΔT_m (ATP-OXA) interaction is comparable with that of the ΔT_m (ATP-IND) interaction. The crystal structure suggests that the stabilizing effect of Mg^{2+} on the interaction

Downloaded from http://www.jbc.org/ at DOE/SC/OSTI on March 11, 2020

between ATP and indolmycin is mediated through the oxazolinone ring, whose orientation is, in turn, stabilized by hydrogen bonds to His^{43} and Gln^{147} as discussed above.

Discussion

An array of crystal structures of both BsTrpRS and H_cTrpRS provide snapshots of the enzymes along their catalytic paths and demonstrate the conformational changes that result from binding of various ligands (12, 13, 24). From these structures, it is evident that H_cTrpRS uses a greater number of binding determinants for tryptophan recognition and that binding of tryptophan causes an induced fit rearrangement of the active site in H_cTrpRS but not BsTrpRS. Here we discuss possible structural and mechanistic reasons for the tight binding of indolmycin to BsTrpRS and the inability of indolmycin to inhibit eukaryotic TrpRSs.

Why Is Indolmycin a High Affinity Inhibitor of Bacterial TrpRS?—There are no drastic global changes between structure 1MAU and the inhibited BsTrpRS structure (Protein Data Bank code 5DK4). We propose that subtle, mechanistically relevant differences in the active site metal configuration account for the ability of indolmycin to inhibit BsTrpRS as tightly as it does. We observe stronger Mg^{2+}-ATP and weaker BsTrpRS-ATP interactions (Fig. 6) as well as altered Mg^{2+} coordination and placement in the inhibited state (indolmycin + Mg^{2+}·ATP; Figs. 3*B* and 4) compared with the pre-transition state (tryptophanamide + Mg^{2+}·ATP) structure. We attribute these differences to the replacement of tryptophanamide with indolmycin that varies mainly at the methylamino-substituted oxazolinone ring of indolmycin. Interactions among His^{43}, Gln^{147}, and indolmycin restrict the oxazolinone ring orientation, thereby reducing the entropy of the α-carbon mimic in the inhibited complex compared with the pre-transition state complex. This unfavorable entropy change is compensated by the enthalpy from additional hydrogen bonds formed among the Mg^{2+}-coordinated water molecules and the oxazolinone nitrogen and carbonyl oxygen atoms as well as the interaction with His^{43}.

These hydrogen bonds stabilize the water molecules that are also tightly coordinated to the catalytic Mg^{2+} ion. Functional groups of the α-carbon atoms of tryptophan and tryptophanamide can adopt alternative conformations that are similar in energy, none of which allow for completion of the Mg^{2+} coordination sphere. We conclude from these observations that completion of that coordination sphere allows the metal to form significantly tighter interactions with all three phosphate oxygen atoms and hence that indolmycin stabilizes a ground state Mg^{2+}·ATP configuration, opposing the tendency of the PreTS state to promote the metal to a high energy state that assists in transition state stabilization.

Furthermore, the oxazolinone ring of indolmycin, stabilized by hydrogen bonds with His^{43} and Gln^{147}, prevents the rotamer switch of Tyr^{125} in the specificity helix that is part of the structural transition from the open to the closed state. To avoid a steric clash with the constrained Tyr^{125} residue, Gln^{107} likewise does not switch rotamers in the presence of indolmycin. Gln^{107} is part of a highly mobile loop that shows a subtle but significant opening in the inhibited state compared with the pre-transition state. This opening results in the weakening of ATP-BsTrpRS interactions, specifically those between Lys^{111} and the γ-phosphate group.

In the catalytically competent PreTS configuration, coordination by lysine residues of the phosphate oxygen atoms promotes the metal to an activated, less stable state with weaker interactions to the three phosphate oxygen atoms and prevents the Mg^{2+} ion from assuming a lower energy position with stronger contacts to ATP. The positively charged Nζ atom of Lys^{111} competes with the Mg^{2+} ion for stabilization of a negatively charged oxygen atom (Oγ) of the γ-phosphate group. In the PreTS state, the Mg^{2+}-Oγ and Lys^{111}-Oγ distances are 2.4 and 2.9 Å, respectively.

Substitution by indolmycin for tryptophanamide simultaneously weakens the Lys^{111}-Oγ (3.4 Å) interaction and strengthens that between that oxygen atom and the Mg^{2+} ion (2.2 Å). Additionally, the 0.4-Å shift in Mg^{2+} placement along with the opening of the mobile loop around Lys^{111} allows for tight, hexavalent Mg^{2+} coordination accompanied by stronger, more nearly equivalent interactions between Mg^{2+} and the three ATP phosphate groups.

Mutation of His^{43} Results in Indolmycin Resistance—When both tryptophanamide and ATP are bound, the His^{43} side chain switches from one rotamer to another in the transition from open to closed PreTS state and back again in the closed product state. This rotamer switch does not occur when the active site is bound to AMP, PP_i, and tryptophan (33). In the PreTS (Mg^{2+}·ATP + LTN) and inhibited (Mg^{2+}·ATP + IND) states, Nϵ2 of His^{43} interacts with Oδ2 of Asp^{132}. In all other observed states, Nϵ2 of His^{43} forms an interaction with the carbonyl oxygen of Tyr^{125}. His^{43} also contributes to indolmycin binding via Nδ1. This reorientation of His^{43} appears to be correlated with the succession of ligands most similar to the putative catalytic reaction path, and it may thus also be functional.

Several groups have identified mutations that confer high level indolmycin resistance (34–36). One of the mutant sites, His^{43}, is of direct interest in the context of the present inhibited structure, which furnishes a semiquantitative explanation for the mutational effects at position 43. We have implicated His^{43} in a hydrogen bond network that requires hydrogen bonds to both indole nitrogen atoms that stabilize the orientation of the plane of the oxazolinone ring of indolmycin. Fixing the orientation of the ring consequently allows formation of a full hexacoordinated environment for the catalytic Mg^{2+} ion, which we have shown accounts for the additional stabilization of the indolmycin·Mg^{2+}·ATP complex.

Indolmycin inhibition of the *B. stearothermophilus* TrpRS H43N mutant is weaker by 3.5 kcal/mol than that of the native enzyme (37). Depending on the stabilization energy provided by these two hydrogen bonds and their coupling, we would predict that an H43N mutant would lose 2–4 kcal/mol binding energy compared with wild-type enzyme. All rotamers of an asparagine substitution at position 43 would result in the loss of two of the three hydrogen bonds observed in the network among indolmycin, His^{43}, and Asp^{132}. Similarly, the homologous H48Q mutation in *Streptomyces coelicolor* similarly appears incapable of forming both hydrogen bonds we observe for His^{43} (36).

Downloaded from http://www.jbc.org/ at DOE/SC/OSTI on March 11, 2020

Modeling Reveals Why Indolmycin Is a Weak Inhibitor of Eukaryotic Cytosolic TrpRS Enzymes—The selectivity ratio of indolmycin for cytosolic *B. taurus* (Bt)TrpRS *versus* BsTrpRS is 10^6-fold in favor of BsTrpRS binding. This selectivity factor far surpasses those of most therapeutic drugs, including trimethoprim (selectivity ratio rat/*Toxoplasma gondii* dihydrofolate reductase, 49) and metoprolol (selectivity ratio β_2/β_1-adrenergic receptor, 6.0), which treat toxoplasmosis and cardiovascular disease, respectively (38, 39). This dramatic selectivity arises by enhancing indolmycin binding recognition by BsTrpRS as we have just shown while reducing eukaryotic cytosolic TrpRS affinity by similar magnitudes. H_cTrpRS shares 93% sequence identity with BtTrpRS and is therefore highly likely to have a comparably weak millimolar affinity for indolmycin. Interest in developing indolmycin as a lead compound for anti-infective therapy as well as the extensive kinetic and structural studies conducted on H_cTrpRS led us to examine the repertoire of deposited H_cTrpRS structures with the purpose of identifying potential means by which eukaryotic cytosolic TrpRS enzymes evade inhibition by indolmycin (13, 14, 40, 41).

Whereas BsTrpRS uses an induced fit mechanism for ATP binding, H_cTrpRS uses induced fit for tryptophan binding. Binding of tryptophan to BsTrpRS is stabilized by one hydrogen bond between the indole nitrogen of tryptophan and Oδ2 of Asp^{132} and π-π interactions with Phe^5. Meanwhile, H_cTrpRS makes seven direct and water-mediated contacts to its tryptophan substrate. The determinants for tryptophan binding to H_cTrpRS include Glu^{199}, which has a direct and water-mediated interaction with the α-amino group of tryptophan (Fig. 7*A*). Modeling of indolmycin into the amino acid binding site introduces steric clashes between indolmycin and Glu^{199} (Fig. 7*B*). Furthermore, Glu^{199} cannot adopt an alternative rotamer conformation without introducing additional clashes between Glu^{199} and Thr^{196}, Trp^{203}, or Phe^{280}. Besides clashing with Glu^{199}, this indolmycin conformer would not form any of the hydrogen bonds observed when tryptophan is bound aside from the bifurcated hydrogen bond with the indole nitrogen, Tyr^{159}, and Gln^{194}. These interactions are preserved because indolmycin was modeled into the active site by overlaying its indole moiety with that of tryptophan (Protein Data Bank code 2QUH).

Indolmycin can be modeled into the active site of H_cTrpRS by rotating the oxazolinone ring away from Glu^{199} to an orientation perpendicular to the indole moiety (Fig. 7*B*). Although this indolmycin conformer does not clash with active site residues, it does disrupt the hydrogen bonding pattern used by the cytosolic enzyme to identify tryptophan as the bound substrate. The α-amino group of tryptophan, which is protonated at physiological pH, is recognized by Glu^{199}, Gln^{284}, and Gln^{313} (Fig. 7*A*). Each of these residues acts a hydrogen bond acceptor, and the negatively charged carboxylate of Glu^{199} forms additional electrostatic interactions with the amino group. According to our model, the side chain amide group of Gln^{284} would act as a hydrogen bond donor for the cyclic oxygen atom in indolmycin that is in the equivalent position of the α-amino group (Fig. 7*B*). Although Glu^{199} cannot form a salt bridge with indolmycin, it can instead share a bifurcated hydrogen bond from the methylamino group nitrogen with Gln^{313}. This nitrogen can accept a hydrogen bond from the hydroxyl group of Tyr^{316}.

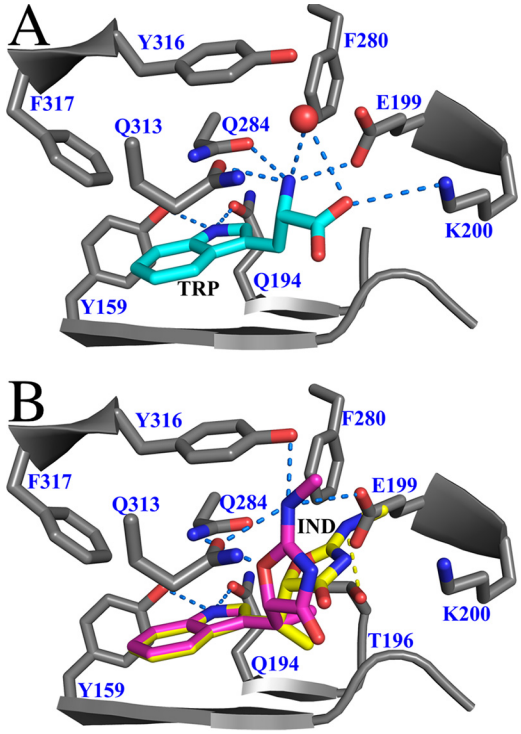

FIGURE 7. **Steric hindrance and altered hydrogen bonding pattern allow H_cTrpRS to discriminate between tryptophan and indolmycin.** *A*, the electrostatic and hydrogen bonding interactions that facilitate specific recognition and binding of Trp to H_cTrpRS (Protein Data Bank code 2QUH) are shown in *yellow dashes*. *B*, IND (*yellow* and *pink sticks*) from the BsTrpRS complex was modeled into the tryptophan binding site of H_cTrpRS (Protein Data Bank code 2QUH) so the indole moieties superimposed. This maintained the H-bonding interactions between the indole nitrogen and Tyr^{159} and Gln^{194}. Rigid body modeling shows that none of the interactions important for tryptophan substrate recognition/binding can form between active site residues and indolmycin (*yellow sticks*). Additionally, rotating the oxazolinone ring away from Glu^{199} eliminates a prominent steric clash between the methylamino group of indolmycin and the side chain carboxylate group of Glu^{199}. This alternate indolmycin conformation (*pink sticks*) allows for more hydrogen bonding interactions between indolmycin and active site residues, although the nature of these interactions is different from those observed upon tryptophan binding. Modeling suggests that these altered interactions allow H_cTrpRS to reject indolmycin as a substrate.

Finally, Lys^{200} cannot form a salt bridge with indolmycin as it does with the tryptophan carboxylate. This electrostatic interaction is also missing when tryptophanamide is bound in place of tryptophan and appears to be critical for progression from the pre-transition state to transition state as this is the only interaction used for tryptophan substrate recognition and binding that cannot form when tryptophanamide occupies the active site. Indolmycin differs from tryptophan by a greater degree than does tryptophanamide. The inability of indolmycin to fully retain the tryptophan-H_cTrpRS side chain interactions, including the salt bridge with Lys^{200}, allows H_cTrpRS to discriminate between tryptophan and the inhibitor. For these reasons, a stable H_cTrpRS·ATP·indolmycin complex is ~1000 less likely to form than that of H_cTrpRS·ATP·tryptophan. Contrastingly, BsTrpRS, which has a 10^3-fold higher affinity for indolmycin over tryptophan, is ~1500 more likely to form a stable, inhibited complex than a catalytically competent tryptophan-bound complex.

Downloaded from http://www.jbc.org/ at DOE/SC/OSTI on March 11, 2020

In this work, we determined the structural basis for high affinity inhibition of BsTrpRS by indolmycin. The simultaneous binding of indolmycin and Mg^{2+}·ATP results in (i) movement of the Tyr^{125} and Gln^{107} side chains, (ii) opening of the mobile loop containing Lys^{111}, (iii) displacement of the Mg^{2+} ion by 0.4 Å, (iv) hexavalent metal coordination, (v) stronger, nearly equivalent electrostatic interactions of Mg^{2+} with an oxygen from each phosphate group of ATP, and (vi) weaker coordination of phosphate group oxygen atoms by active site lysine residues. These changes are reinforced by the hydrogen bonding interactions of Gln^{147}, His^{43}, and Mg^{2+}-coordinated water molecules with indolmycin. We propose that weaker coordination by lysine residues of the phosphate oxygen atoms and stronger Mg^{2+}-ATP interactions induced by indolmycin binding allow the Mg^{2+} ion to settle into a lower energy state, thereby significantly increasing affinity by preventing activation of the metal required for use in amino acid activation.

Author Contributions—C. W. C. and T. L. W. conceived the experimental plan based on previous work by Y. W. Y., T. L. W. carried out all experimental work, analyzed the data, and wrote the paper in consultation with C. W. C. and Y. W. Y.

Acknowledgments—We are grateful to D. Söll and to J. Sello for discussions and unpublished data on indolmycin-resistant mutants of E. coli and indolmycin-resistant TrpRS variants in S. griseus. Shubin Liu kindly performed quantum mechanical simulations of Mg^{2+}·ATP.

References

1. Werner, R. G., Thorpe, L. F., Reuter, W., and Nierhaus, K. H. (1976) Indolmycin inhibits prokaryotic tryptophanyl-tRNA ligase. *Eur. J. Biochem.* **68,** 1–3
2. Ogilvie, A., Wiebauer, K., and Kersten, W. (1975) Inhibition of leucyl-transfer ribonucleic acid synthetasymol. *Biochem. J.* **152,** 511–515
3. Nakama, T., Nureki, O., and Yokoyama, S. (2001) Structural basis for the recognition of isoleucyl-adenylate and an antibiotic, mupirocin, by isoleucyl-tRNA synthetase. *J. Biol. Chem.* **276,** 47387–47393
4. Konrad, I., and , R. (1977) Inhibition of phenylalanine tRNA synthetase from *Bacillus subtilis* by ochratoxin A. *FEBS Lett.* **83,** 341–347
5. Sutherland, R., Boon, R. J., Griffin, K. E., Masters, P. J., Slocombe, B., and White, A. R. (1985) Antibacterial activity of mupirocin (pseudomonic acid), a new antibiotic for topical use. *Antimicrob. Agents Chemother.* **27,** 495–498
6. Kanamaru, T., (2001) *In vitro* and *in vivo* antibacterial activities of TAK-083, an agent for treatment of *Helicobacter pylori* infection. *Antimicrob. Agents Chemother.* **45,** 2455–2459
7. Werner, R. G., and Reuter, W. (1979) Interaction of indolmycin in the metabolism of tryptophan in rat liver. *Arzneimittelforschung* **29,** 59–63
8. Weinreb, V., Li, L., Campbell, C. L., Kaguni, L. S., and Carter, C. W., Jr. (2009) Mg^{2+}-assisted catalysis by *B. stearothermophilus* TrpRS is promoted by allosteric effects. *Structure* **17**, 952–964
9. Retailleau, P., Weinreb, V., Hu, M., and Carter, C. W., Jr. (2007) Crystal structure of tryptophanyl-tRNA synthetase complexed with adenosine-5′ tetraphosphate: evidence for distributed use of catalytic binding energy in amino acid activation by class I aminoacyl-tRNA synthetases. *J. Mol. Biol.* **369**, 108–128
10. Weinreb, V., Li, L., and Carter, C. W., Jr. (2012) A master switch couples Mg^{2+}-assisted catalysis to domain motion in *B. stearothermophilus* tryptophanyl-tRNA Synthetase. *Structure* **20**, 128–138
11. Zhou, M., Dong, X., Shen, N., Zhong, C., and Ding, J. (2010) Crystal structures of *Saccharomyces cerevisiae* tryptophanyl-tRNA synthetase: new insights into the mechanism of tryptophan activation and implications for anti-fungal drug design. *Nucleic Acids Res.* **38,** 3399–3413
12. Retailleau, P., Vonrhein, C., Bricogne, G., Roversi, P., Ilyin, V., and Carter, C. W., Jr. (2003) Interconversion of ATP binding and conformational free energies by tryptophanyl-tRNA synthetase: structures of ATP bound to open and closed, pre-transition-state conformations. *J. Mol. Biol.* **325,** 39–63
13. Shen, N., Zhou, M., Yu, Y., Dong, X., and Ding, J. (2008) Catalytic mechanism of the tryptophan activation reaction revealed by crystal structures of human tryptophanyl-tRNA synthetase in different enzymatic states. *Nucleic Acids Res.* **36,** 1288–1299
14. Yang, X. L., McRee, D. E., and Schimmel, P. (2007) Functional and crystal structure analysis of active site adaptations of a potent anti-angiogenic human tRNA synthetase. *Structure* **15,** 793–805
15. Studier, F. W. (2005) Protein production by auto-induction in high density shaking cultures. *Protein Expr. Purif.* **41,** 207–234
16. Fersht, A. R., Ashford, J. S., Bruton, C. J., Jakes, R., Koch, G. L., and Hartley, B. S. (1975) Active site titration and aminoacyl adenylate binding stoichiometry of aminoacyl-tRNA synthetases. *Biochemistry* **14,** 1–4
17. Francklyn, C. S., First, E. A., Perona, J. J., and Hou, Y. M. (2008) Methods for kinetic and thermodynamic analysis of aminoacyl-tRNA synthetases. *Methods* **44,** 100–118
18. Schneider, C. A., Rasband, W. S., and Eliceiri, K. W. (2012) NIH Image to ImageJ: 25 years of image analysis. *Nat. Methods* **9,** 671–675
19. SAS Institute (2013) *JMP: The Statistical Discovery Software*, SAS Institute, Cary, NC
20. Kabsch, W. (2010) XDS. *Acta Crystallogr. D Biol. Crystallogr.* **66,** 125–132
21. Adams, P. D., Afonine, P. V., Bunkóczi, G., Chen, V. B., Davis, I. W., Echols, N., Headd, J. J., Hung, L. W., Kapral, G. J., Grosse-Kunstleve, R. W., McCoy, A. J., Moriarty, N. W., Oeffner, R., Read, R. J., Richardson, D. C., Richardson, J. S., Terwilliger, T. C., and Zwart, P. H. (2010) PHENIX: a comprehensive Python-based system for macromolecular structure solution. *Acta Crystallogr. D Biol. Crystallogr.* **66,** 213–221
22. Emsley, P., Lohkamp, B., Scott, W. G., and Cowtan, K. (2010) Features and development of Coot. *Acta Crystallogr. D Biol. Crystallogr.* **66,** 486–501
23. Cleland, W. W., and Northrop, D. B. (1999) Energetics of substrate binding, catalysis, and product release. *Methods Enzymol.* **308,** 3–27
24. Ilyin, V. A., Temple, B., Hu, M., Li, G., Yin, Y., Vachette, P., and Carter, C. W., Jr. (2000) 2.9Å crystal structure of ligand-free tryptophanyl-tRNA synthetase: domain movements fragment the adenine nucleotide binding site. *Protein Sci.* **9,** 218–231
25. Doublié, S. (1993) *2.9 Å Crystal Structure of Bacillus stearothermophilus Tryptophanyl-tRNA Synthetase Complexed to its Adenylate, Tryptophanyl-5′AMP*. Ph.D. thesis, University of North Carolina at Chapel Hill
26. Retailleau, P., Yin, Y., Hu, M., Roach, J., Bricogne, G., Vonrhein, C., Roversi, P., Blanc, E., Sweet, R. M., and Carter, C. W., Jr. (2001) High resolution experimental phases for tryptophanyl-tRNA synthetase (TrpRS) complexed with tryptophanyl-5′AMP. *Acta Crystallogr. D Biol. Crystallogr.* **57,** 1595–1608
27. Yin, Y. (1995) *Crystallographic Study of Bacillus stearothermophilus tryptophanyl-tRNA synthetase in its catalytic reaction*. Ph.D. thesis, University of North Carolina at Chapel Hill
28. Calvin, M., Hermans, J., Jr., and Scheraga, H. A. (1959) Effect of deuterium on the strength of hydrogen bonds. *J. Am. Chem. Soc.* **81,** 5048–5050
29. Matulis, D., Kranz, J. K., Salemme, F. R., and Todd, M. J. (2005) Thermodynamic stability of carbonic anhydrase: measurements of binding affinity and stoichiometry using thermofluor. *Biochemistry* **44,** 5258–5266
30. Niesen, F. H., Berglund, H., and Vedadi, M. (2007) The use of differential scanning fluorimetry to detect ligand interactions that promote protein stability. *Nat. Protoc.* **2,** 2212–2221
31. Weber, P. C., Wendoloski, J. J., Pantoliano, M. W., and Salemme, F. R. (1992) Crystallographic and thermodynamic comparison of natural and synthetic ligands bound to streptavidin. *J. Am. Chem. Soc.* **114,** 3197–3200
32. Jencks, W. P. (1981) On the attribution and additivity of binding energies. *Proc. Natl. Acad. Sci. U.S.A.* **78,** 4046–4050
33. Laowanapiban, P., Kapustina, M., Vonrhein, C., Delarue, M., Koehl, P., and Carter, C. W., Jr. (2009) Independent saturation of three TrpRS subsites generates a partially assembled state similar to those observed

Downloaded from http://www.jbc.org/ at DOE/SC/OSTI on March 11, 2020

in molecular simulations. *Proc. Natl. Acad. Sci. U.S.A.* **106,** 1790–1795
34. Kitabatake, M., Ali, K., Demain, A., Sakamoto, K., Yokoyama, S., and Söll, D. (2002) Indolmycin resistance of *Streptomyces coelicolor* A3(2) by induced expression of one of its two tryptophanyl-tRNA synthetases. *J. Biol. Chem.* **277,** 23882–23887
35. Hurdle, J. G., O'Neill, A. J., and Chopra, I. (2004) Anti-staphylococcal activity of indolmycin, a potential topical agent for control of staphylococcal infections. *J. Antimicrob. Chemother.* **54,** 549–552
36. Vecchione, J. J., and Sello, J. K. (2009) A novel tryptophanyl-tRNA synthetase gene confers high-level resistance to indolmycin. *Antimicrob. Agents Chemother.* **53,** 3972–3980
37. Ali, K. S. (2002) *Bacillus stearothermophilus Tryptophanyl-tRNA Synthetase: Mutations Leading to Indolmycin Resistance.* Ph.D. thesis, Yale University
38. Gangjee, A., Vasudevan, A., Queener, S. F., and Kisliuk, R. L. (1996) 2,4-Diamino-5-deaza-6-substituted pyrido[2,3-d]pyrimidine antifolates as potent and selective nonclassical inhibitors of dihydrofolate reductases. *J. Med. Chem.* **39,** 1438–1446
39. Smith, C., and Teitler, M. (1999) β-Blocker selectivity at cloned human β1- and β2-adrenergic receptors. *Cardiovasc. Drugs Ther.* **13,** 123–126
40. Yang, X. L., Otero, F. J., Skene, R. J., McRee, D. E., Schimmel, P., and Ribas de Pouplana, L. (2003) Crystal structures that suggest late development of genetic code components for differentiating aromatic side chains. *Proc. Natl. Acad. Sci. U.S.A.* **100,** 15376–15380
41. Yu, Y., Liu, Y., Shen, N., Xu, X., Xu, F., Jia, J., Jin, Y., Arnold, E., and Ding, J. (2004) Crystal structure of human tryptophanyl-tRNA synthetase catalytic fragment: insights into substrate recognition, tRNA binding, and angiogenesis activity. *J. Biol. Chem.* **279,** 8378–8388

Downloaded from http://www.jbc.org/ at DOE/SC/OSTI on March 11, 2020

Selective Inhibition of Bacterial Tryptophanyl-tRNA Synthetases by Indolmycin Is Mechanism-based

Tishan L. Williams, Yuhui W. Yin and Charles W. Carter, Jr.

J. Biol. Chem. 2016, 291:255-265.
doi: 10.1074/jbc.M115.690321 originally published online November 9, 2015

Access the most updated version of this article at doi: 10.1074/jbc.M115.690321

Alerts:
- When this article is cited
- When a correction for this article is posted

Click here to choose from all of JBC's e-mail alerts

This article cites 37 references, 10 of which can be accessed free at
http://www.jbc.org/content/291/1/255.full.html#ref-list-1

Downloaded from http://www.jbc.org/ at DOE/SC/OSTI on March 11, 2020